PREDICTION OF THE CONTACT THERMAL RESISTANCE OF VERTICAL CARBON NANOTUBE ARRAYS

by

Bo SHI*, Han ZHANG, and Jin ZHANG

Jiangsu Province Key Laboratory of Aerospace Power System,
College of Energy and Power Engineering,
Nanjing University of Aeronautics and Astronautics, Nanjing, China

Original scientific paper
https://doi.org/10.2298/TSCI180625289S

The vertical carbon nanotube arrays (VACNT), as a result of its flexibility and axial high thermal conductivity, exert a huge potential and play an increasingly important role in thermal interface materials. This paper proposed a model which can predict the contact thermal resistance of VACNT. The contact thermal resistance of VACNT under different pressures is calculated and compared with the experimental data. Also, the effect of variations in the surface roughness and VACNT parameters on the contact thermal resistance is investigated. Results show that the theoretical results are in good agreement with the experimental data. The contact thermal resistance is composed of interfacial thermal resistance, constriction thermal resistance, and VACNT resistance. Among which the interfacial thermal resistance is the major thermal resistance. The variations in VACNT length and diameter can change the bending degree of VACNT under the same pressure, which presents important implications on contact thermal resistance and can be used to optimize the contact thermal resistance of VACNT. The surface roughness exerts little effect on contact thermal resistance.

Key words: *VACNT parameters, contact thermal resistance, surface roughness, interfacial thermal resistance vertical carbon nanotube arrays*

Introduction

As early as 2000, Intel Corporation announced that the chip dissipation problem of the personal computer has restricted its power to further improvement [1]. The traditional heat dissipation technique is to transfer the chip heat directly or through the vapor chamber to a heat sink with strong heat dissipation capability. However, the chip and heat sink are mainly connected by solid-solid contact method. The roughness makes the actual contact area small and introduces the contact thermal resistance, which becomes critical in high heat flux.

The use of thermal interface materialis (TIM) is a most effective method to reduce the thermal resistance between two contact interfaces. However, the commonly used TIM, such as thermal grease, thermal gasket and phase change materials, has a very low effective thermal conductivity. More seriously, the life and reliability of electronic devices will be seriously affected by its problems of aging, failure and leakage. The CNT, ever since it was proved to have high thermal conductivity and strong thermal stability, is the best candidate for adapting to the increasing power of electronics, and can be used to improve the property of TIM [2-4].

* Corresponding author, e-mail: boshi@nuaa.edu.cn

Many scholars have conducted a series of studies on its performance [5-7]. Wang *et al.* [8] fabricated a bilayer aligned CNT-TIM and found that it could effectively reduce the overall thermal resistance of the TIM to 8.78 mm^2K/W. Khanh *et al.* [9] measured the thermal resistances of VACNT using two polymers and found that the reactive polymers, which was able to establish covalent bonds with the CNT, could greatly reduce the thermal resistance. Xu and Fisher [10] found that the addition of the CNT arrays as TIM could reduce the resistance under moderate load compared to the indium sheet and phase-change TIM, with a minimum resistance of 19.8 mm^2K/W at a pressure of 0.445 MPa. Li *et al.* [11] found that the contact resistance of CNT-polymer was lower compared to the CNT-metal. Hirotani *et al*. [12] measured the interfacial thermal resistance (ITR) between the VACNT and SiO_2 surface and found that the ITR between the VACNT tip and the SiO_2 surface was independent of contact pressure. To improve the in-plane thermal conduction of VACNT arrays, Kong *et al.* [13] proposed a 3-D CNT network structure and found that the in-plane thermal conductivity is 5.40 ±0.92 W/mK, nearly 30 times higher than the VACNT arrays. Kaur *et al.* [14] connected the metal surfaces and VACNT with short, covalently bonded organic molecules to enhance thermal transport at the interface and showed a sixfold reduction in the thermal interface resistance. Sun *et al.* [15] also experimentally demonstrated that it can improve thermal transport between the VACNT and graphene hybrid material interfaces by Covalent Bonds.

The previous researches on the performance of VACNT are experimental oriented. Based on the experimental results and mathematical analysis, many scholars proposed a number of models and assumptions to calculate the contact thermal resistance and began to carry out theoretical research. Hu *et al.* [16] studied the effects of the crossing angle, nanotube length and initial nanotube spacing on the thermal resistance of the crossed CNT by the non-equilibrium molecular dynamics (MD) method, founding that the thermal resistance increases with the increase of crossing angle and initial nanotube spacing, while decreases with the increasing nanotube length. Yovanovich *et al.* [17] proposed a CMY plastic contact thermal resistance model, which indicated that the surface asperities are satisfied with the Gaussian distribution. By comparing the surface asperities with the particles in statistical thermodynamics, Leung *et al.* [18] studied the contact thermal resistance and its interaction mechanism. However, there is few satisfactory theoretical model to predict the thermal resistance of various conditions, and the empirical formula for describing the effects of various factors such as VACNT parameters and surface roughness on contact thermal resistance is still unclear.

In this paper, a model which can predict the thermal contact resistance of the VACNT is proposed. It presents a complete description from contact analysis to the calculation of the contact thermal resistance. The theoretical results are compared with the experimental date. Also, the effect of variations in the surface roughness and CNT parameters on the contact thermal resistance is studied particularly, with the aim of obtaining some useful information for optimizing the contact thermal resistance of VACNT.

Model description

The contact of two rough surfaces can be simplified to the contact between a randomly rough surface and a rigid smooth surface [19]. As shown in fig. 1, a rough copper surface is contact with a smooth Si surface which is grown with VACNT on it. Without VACNT, incomplete contact between two surfaces caused by the roughness of the copper surface will lead to the heat flow contraction, resulting in high contact thermal resistance. While the VACNT are deposited on it, the contact area is greatly enhanced due to the flexibility of VACNT, and at the same time, the contact thermal resistance is greatly reduced.

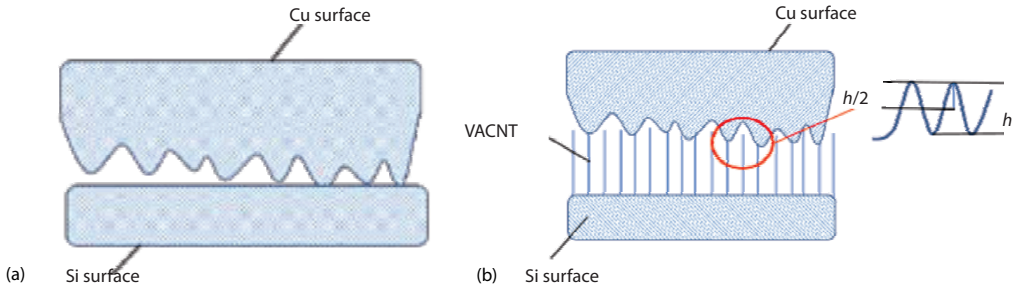

Figure 1. Contact between; (a) the copper surface and Si surface, (b) VACNT as TIM

Mechanical analysis of CNT

Many scholars have studied the mechanical properties of CNT and indicated that the macroscopic mechanical model could be applied to calculate its mechanical properties [20, 21]. In this paper, the CNT is considered as a elastic rod with initial curvature. The force diagram of the rod is shown in fig. 2. Liu [22] deduced the flexible line equation of the compressed straight rod in Cartesian co-ordinate system, which is derived from the curve co-ordinates. And it is applied to calculate the force of the CNT.

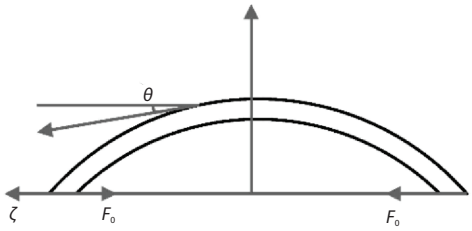

Figure 2. The force diagram of a rod

Force of the CNT is calculated:

$$F_0 = 4EI / L^2 \left(\int_0^{\pi/2} \frac{\mathrm{d}\varphi}{\sqrt{1-k^2 \sin^2 \varphi}} \right) \tag{1}$$

where

$$\sin\varphi = \frac{\sin\dfrac{\theta}{2}}{k}, \quad k = \sin\frac{\theta_0}{2}$$

and $E = 1$, F_0 is the force of the CNT with initial curvature, E – is the Young's modulus of CNT.

Axial displacement of the CNT:

$$\xi(\varphi) = \frac{L}{2\displaystyle\int_0^{\pi/2} \frac{\mathrm{d}\varphi}{\sqrt{1-k^2 \sin^2 \varphi}}} \left(\int_0^{\varphi} \frac{1-2k^2 \sin^2 \varphi}{\sqrt{1-k^2 \sin^2 \varphi}} \mathrm{d}\varphi \right) \tag{2}$$

Equations (1) and (2) include an elliptic integral, which makes it difficult to calculate the analytical solution. In this paper, the numerical solution is applied to find the results of the eqs. (1) and (2).

Analysis of surface roughness

In the contact process, the actual contact occurs only on a small number of discrete asperities due to the influence of roughness. Studies show that the asperity distribution of most rough surfaces is random and close to Gaussian distribution, and the deformation of asperity

in the process of contact can be considered to be elastic [23, 24]. The effect of roughness on the contact resistance of VACNT is considered in this model as well, which is described by Greenwood and Williamson's model (GW). The GW model uses a parabolic function describe the peak. The peak height on the midpoint is corresponding to the Gaussian distribution [25]:

$$\phi(z) = \frac{1}{\sqrt{2\pi}\sigma}\exp\left(-\frac{z^2}{2\sigma^2}\right) \tag{3}$$

where $\sigma = \sigma_1^2 + \sigma_2^2$ is the equivalent roughness of the contact surfaces.

When the Si surface is in direct contacted with the copper surface, the contact area between them is much smaller than the nominal contact area and the peak parts are the major influencing factors. While the VACNT are used as the TIM, the contact area in the valley parts becomes larger and the valley parts should be considered. Therefore, a convex model is proposed in our work, assuming that the peak height is constant. The shape of the convex is shown in fig. 1(b), the enlarged image in the red circle. When dealing with the contacting surfaces, two reference planes are defined. One is the mean of the asperity heights and the other is the mean of the copper surface heights, as shown in fig. 3.

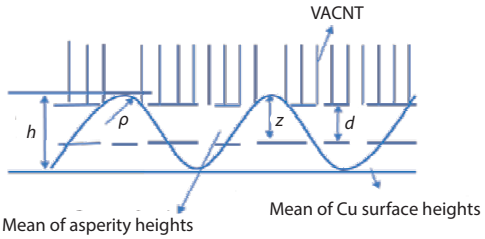

Figure 3. The basic geometry model of contacting surfaces

In the case of contact model analysis, there assumptions are hypothesized as discussed in many articles [26]:

– The radius of curvature of the asperity is same.
– The height of the asperity satisfies Gaussian distribution.
– The contact between the asperities is elastic.

The peak height can be calculated:

$$h = \frac{1}{4\pi\rho\eta} \tag{4}$$

where $\rho = \rho_1\rho_2/(\rho_1 + \rho_1)$ is the equivalent peak curvature.

According to the aforementioned assumptions, the shape of the asperities is ultimately determined by three parameters: σ, ρ , and η. The deformation of the asperities is neglected in this paper considering that its deformation is much smaller than that of CNT.

The specific calculation steps of the model:

The total number of asperities in contact:

$$N_c = \eta A_n \int_d^\infty \phi(z)\,\mathrm{d}z \tag{5}$$

Define the normal deformation:

$$w = z - d \tag{6}$$

During loading, the contact area, A_e, and the contact force, F_e, of each individual asperity are only related to the deformation of the asperities, w, when it is assumed that there is no interference between asperities. That is to say:

$$A_e = A(w), \quad F_e = F(w) \tag{7}$$

Then the total contact area and contact pressure are calculated:

$$A(d) = \eta A_{\mathrm{n}} \int_{d}^{\infty} A_{\mathrm{e}}(z-d)\phi(z)\,\mathrm{d}z$$
$$P(d) = \eta \rho_{\mathrm{cnt}} \int_{d}^{\infty} F_{\mathrm{e}}(z-d)\phi(z)\,\mathrm{d}z \tag{8}$$

The function that describes the profile of the peak is a piecewise function, so $A_e(w)$ and $F_e(w)$ are also piecewise function and its expression is:

$$A_{\mathrm{e}}(w) = \begin{cases} 2\pi\rho w, \left(w \le \dfrac{h}{2}\right) \\ \left(\dfrac{1}{\eta} - 2\pi\rho h\right) + 2\pi\rho w, \left(\dfrac{h}{2} < w \le h\right) \\ \dfrac{1}{\eta}, (w > h) \end{cases} \tag{9}$$

$$F_{\mathrm{e}}(w) = \begin{cases} \displaystyle\int_0^{\sqrt{2\pi w/\rho}} \left(\frac{F_0 w - F_0 \rho x^2}{2}\right) \pi x \mathrm{d}x, \quad \left(w \le \frac{h}{2}\right) \\ \displaystyle\int_0^{\sqrt{\pi h/2\rho}} \left(\frac{F_0 w - F_0 \rho x^2}{2}\right) \pi x \mathrm{d}x \\ \quad + \displaystyle\int_{\sqrt{\pi h/2\rho}}^{\sqrt{\pi h/\rho} - \sqrt{2(w+d)/\rho}} \left[F_0 w - F_0 h + F_0 \rho \left(\frac{x - \sqrt{\dfrac{\pi h}{\rho}}}{2}\right)\right] \pi x \mathrm{d}x, \left(\dfrac{h}{2} < w \le h\right) \\ \displaystyle\int_0^{\sqrt{\pi h/2\rho}} \left(F_0 w - \frac{F_0 \rho x^2}{2}\right) \pi x \mathrm{d}x + \int_{\sqrt{\pi h/2\rho}}^{\sqrt{\pi h/\rho}} \left[F_0 w - F_0 h + F_0 \rho \left(\frac{x - \sqrt{\dfrac{\pi h}{\rho}}}{2}\right)\right] \pi x \mathrm{d}x), \ (w > h) \end{cases} \tag{10}$$

Contact resistance calculation

The contact thermal resistance is composed of three mainly parts: the ITR which is caused by the difference of the phonon spectrum and the electron spectrum between the VACNT and the copper surface, and the constriction thermal resistance which is caused by the incomplete contact, as well as the thermal resistance of CNT.

The thermal resistance network for the model is shown in fig. 4. The total thermal resistance:

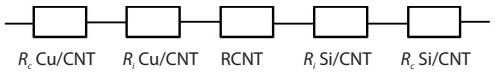

Figure 4. The thermal resistance network for the model

$$R_{\mathrm{total}} = R_{\mathrm{c\,Cu/CNTs}} + R_{\mathrm{i\,Cu/CNTs}} + R_{\mathrm{CNTs}} + R_{\mathrm{i\,Si/CNTs}} + R_{\mathrm{c\,Si/CNTs}} \tag{11}$$

In which, $R_{\mathrm{cCu/CNTs}}$ and $R_{\mathrm{cSi/CNTs}}$ are the constriction thermal resistance of Cu-CNT and Si-CNT, respectively, $R_{\mathrm{iCu/CNTs}}$ and $R_{\mathrm{iSi/CNTs}}$ are the ITR of Cu-CNT and Si-CNT, respectively, and is the thermal resistance of the VACNT.

In the calculation of the contact resistance model, assuming that there is no heat loss during contact, all heat flows are transferred by contact between solids and the physical parameters are constant during heat transfer [27].

Interfacial thermal resistance

Many scholars have used MD to study the interface resistance and heat transfer characteristics between CNT and the target surface, which is also used in this paper.

The Tersoff potential energy is used to describe the interaction between carbon atoms and silicon atoms, as many scholars have done [28, 29]. The embedded atom met (EAM) potential is applied to simulate the interaction between copper atoms [30, 31]. And the Lennard-Jones potential energy is selected to describe the interaction between copper and carbon atoms in view of the fact that many scholars have adopted van der Waals in [32].

The ITR is composed of the Cu-CNT ITR and the Si-CNT ITR. As mentioned in the previous paragraph, the interaction in carbon atoms and silicon atoms are all the Tersoff potential, which indicates that the silicon and carbon atoms are tightly connected with each other when in direct contact just like the same atoms, therefore, the Si-CNT ITR can be considered very small, far less than the Si-CNT ITR, and can be omitted in calculation.

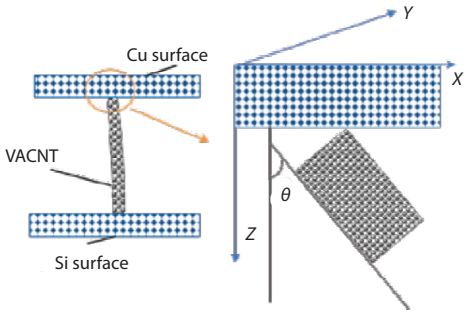

Figure 5. The interface models in Cu-CNT-Si structure

The Cu-CNT ITR, which is caused by the mismatch of the CNT and the copper lattice, is calculated by the MD. Figure 5 shows the interface models simulated between CNT and copper crystal. The upper part is *fcc* copper crystal with bottom surface (001). The lower part is (10, 10) CNT structure. The contact angle, θ, between the CNT and the copper surface is the angle between the axis of the CNT and the nominal direction of the copper surface. Periodic boundary condition is used in the *X*- and *Y*-directions.

The ITR of single CNT contacted with copper lattice [33]:

$$r_{\mathrm{i}} = \frac{\Delta T}{Q} \tag{12}$$

This paper assumes that r_{i} is only depended on the contact angle. The ITR of the whole surface can be calculated:

$$R_{\mathrm{i\,Cu/CNTs}} = A_{\mathrm{n}} \sum\nolimits_{\theta} \left[\frac{r_{\mathrm{i}}(\theta)}{n_{\mathrm{i}}(\theta)} \right] \tag{13}$$

Constriction thermal resistance

The constriction resistance is caused by the constriction of heat flow at the rough contact surface. When the VACNT are used as the TIM, the constriction thermal resistance is the sum of the Cu-CNT constriction thermal resistance and the Si-CNT constriction thermal resistance. The length of the VACNT is much smaller compared to the incomplete contact gap between the two contact surfaces, therefore, it can be simplified to the calculation of the constriction thermal resistance in Cu-Si surfaces.

The individual constriction thermal resistance per unit area can be described [34]:

$$r_c = \frac{\left(\frac{1-a}{b}\right)^{1.5}}{2ak_e} \tag{14}$$

where

$$a = \sqrt{\frac{A(d)}{\pi N_c}},\ b = \sqrt{\frac{A_n}{\pi N_c}},\ k_e = \frac{k_1 k_2}{k_1 + k_2}$$

is the equivalent thermal conductivity.

Total constriction resistance can be calculated:

$$R_c = R_{c\,Cu/CNTs} + R_{c\,Si/CNTs} = \frac{A_n r_c}{N_c} \tag{15}$$

Thermal resistance of VACNT

When the heat goes through the VACNT, the thermal resistance generated by the heat transfer between the CNT and the CNT-defects will result in the thermal resistance of CNT. Previous work show that the thermal conductivity of CNT varies from hundreds to thousands W/mK. Eric *et al.* [35] stated that the thermal conductivity of SWCNT was close to 3500 W/mK. Fujii *et al.* [36] found that when the CNT-diameter was 16.1 nm, the axial thermal conductivity of the CNT was about 1800 W/mK at room temperature. Bi *et al.* [37] concluded that the thermal conductivity of SWCNT was about 600 W/mK with the length of the SWCNT varying from 2.5-25 nm. They also pointed out that the high thermal conductivity of CNT was mainly determined by phonon Heat conduction rather than electronic heat conduction.

The thermal resistance of CNT is described as:

$$R_{CNTs} = \frac{\left(\frac{L}{k_c A_c}\right)}{N} \tag{16}$$

The thermal resistance of the CNT under different thermal conductivity is calculated according to the parameters in tab. 2 and the results are shown in tab. 1.

Table 1. Thermal resistance of CNT

k_c = 600 [Wm^{-1}K^{-1}]			k_c = 3500 [Wm^{-1}K^{-1}]		
P	R_{total}	R_{CNTs}	P	R_{total}	R_{CNTs}
0.31	43.77	2.22	0.31	41.93	0.38
0.27	50.56	2.56	0.27	48.45	0.44
0.23	58.78	2.97	0.23	56.32	0.51
0.20	68.75	3.47	0.20	65.88	0.60
0.17	80.93	4.07	0.17	77.55	0.70

Table 2. Specific calculation parameters

Calculation parameters			
Parameters of roughness		Parameters of VACNT	
σ [μm]	1	D [nm]	50
ρ [μm]	150	L [μm]	12
η [mm^2]	350	ρ_{cnt} [μm^{-2}]	200
k_c [Wm^{-1}K^{-1}]	104	k_c [Wm^{-1}K^{-1}]	2000

When the thermal conductivity of CNT varies from 600-3500 W/mK, the thermal resistance of the CNT has a slight decrease and is much smaller compared to the total thermal resistance. The variations in thermal conductivity of CNT have little impact on the total thermal resistance. In this paper, we choose k_c = 2000 W/mK as the thermal conductivity of CNT.

Results and discussion

According to the aforementioned description, a computer program was developed to solve the results numerically. The thermal contact resistance under various pressures is calculated and compared to the experimental results. The influence of the peak curvature, the number of asperities per unit area, the standard deviation of the peak distribution, and the influence of the CNT-length, diameter and density on the thermal resistance are analyzed, respectively.

Comparison with experimental data

Xu and Fisher [38] measured the contact thermal resistance between a copper surface and a silicon surface which is grown with CNT on it. The contact thermal resistance for the uncoated control sample (a sample that without the CNT as TIM is also included for comparison. The surface roughness of Si and Cu are 0.09 and 1 and the thermal conductivities for Cu and Si take constant values of 391.1 W/mK and 141 W/mK , respectively.

With the previous parameters, the equivalent roughness and thermal conductivity can be obtained. The specific calculation parameters needed in this paper are shown in tab. 2. Then the computational procedure was run to construct the results.

Figure 6 shows the comparative results between the present model and the experimental data of Xu and Fisher [38]. It can be seen that the theoretical results are in good agreement with the experimental data. As the pressure increases, the thermal resistance decreases and tends to be flat. With high-quality VACNT, the thermal resistance in present model is two to three times lower than the values of the bare wafer (without CNT between Cu-Si surfaces), which demonstrates that the adoption of the CNT as TIM can largely reduce the thermal resistance between the contact surfaces.

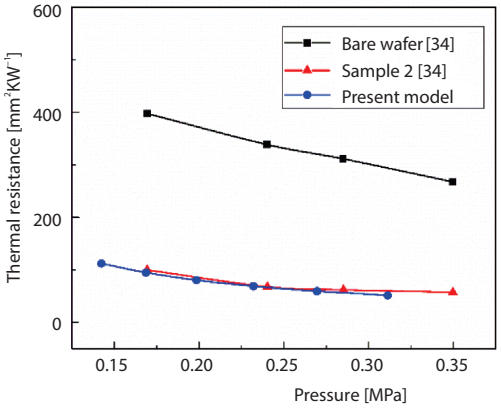

Figure 6. Comparison of present model with experimental date of [38]

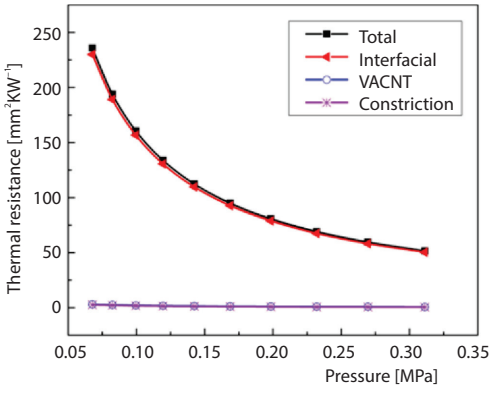

Figure 7. Contact thermal resistance of present model as a function of pressure

Figure 7 shows the contact hermal resistance as a function of pressure. The contact thermal resistance composes three thermal resistances: the ITR, the constriction thermal resistance, as well as the thermal resistance of CNT. It can be seen that all the three thermal resistances are inversely proportional to the pressure, that is, with the pressure increasing, the three thermal resistances tend to decrease. The effect of constriction resistance and VACNT resistance on contact resistance can be neglected and the total thermal resistance is determined only by the ITR. Therefore, the ITR is the major thermal resistance.

The point contact between the VACNT tips and the copper surface results in a decrease in the actual contact area, which is the major cause of the larger ITR. Applying thermal grease/gels or phase change materials (PCM) to the interfaces can create more heat flow path between the VACNT and the target surface, which might significantly reduce the ITR.

The influence of the VACNT parameters on contact thermal resistance

Figure 8 shows the influence of the VACNT parameters on contact thermal resistance. With the VACNT length increased and the VACNT diameter declined, the slope of the total thermal resistance-pressure curve increases, which indicates that the influence of pressure on the total thermal resistance becomes stronger. The increase of the VACNT length and the decline of the VACNT diameter makes it easier for VACNT to compress under the same pressure and becomes bent. The bending of the VACNT increases the heat transfer area between the VACNT and the copper surface in the whole VACNT arrays, resulting in the heat conduction channel raised and the total thermal resistance reduced, which can be used to account for the result shown in figs. 8(a) and 8(b). When the pressure is from 0.15-0.35 MPa, there is a little bit increase in total thermal resistance as the VACNT density increases. Because the increase in VACNT density makes the point contact between the VACNT tips and the copper surface increase, but at the same time, it also makes the VACNT difficult to compress. The heat transfer area between the VACNT and the copper surface which is caused by the bending of the VACNT will decrease, resulting in the heat transfer channel reduced and the total thermal resistance raised.

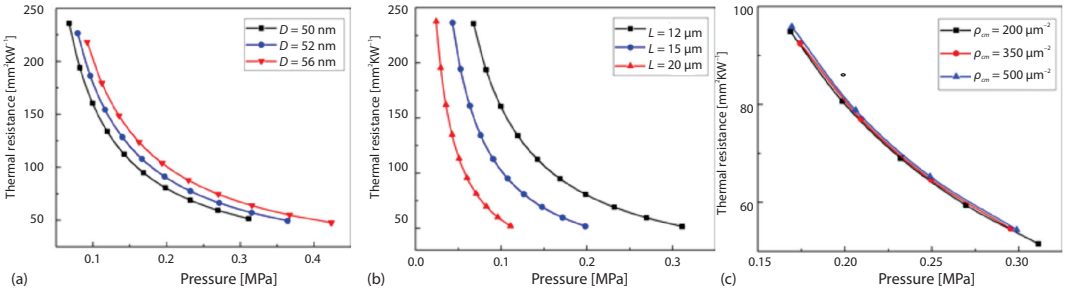

Figure 8. The influence of (a) the VACNT diameter, (b) the VACNT length, and (c) the VACNT density on contact thermal resistance

Therefore, the bending degree of VACNT has important implications on the total thermal resistance. As the bending degree enhanced, the total thermal resistance will decrease gradually. When the VACNT density is determined, the contact thermal resistance can be reduced by increasing the VACNT length or by reducing the VACNT diameter.

The influence of the roughness on contact thermal resistance

As can be seen from the analysis of surface roughness described by GW model in section *Analysis of surface roughness*, the roughness is mainly determined by the standard deviation of the peak distribution and the peak height which is subject to the peak curvature and the number of asperities per unit area. The influence of these three factors on the roughness is shown in fig. 9. Figures 9(a) and 9(b) illustrate the influence of the peak height on contact thermal resistance. With the increase of the peak curvature and the number of asperities per unit

area, the total thermal resistance is almost unchanged, indicating that the peak height, that is, the shape of the peaks has little effect ontal thermal resistance.

The determining factor affecting roughness is the standard deviation of the peak distribution. As it increases, the total thermal resistance exhibits a slight increase, as shown in fig. 9(c). With the standard deviation of the Gaussian distribution increasing, the copper surface gets rougher. When it is subject to different pressures, the contact area between the copper surface and the VACNT will decrease, resulting in a reduction in the heat conduction channels and a slight raise in total thermal resistance. From the aforementioned analysis, we can draw the conclusion that the surface roughness exerts little effect on the total contact thermal resistance.

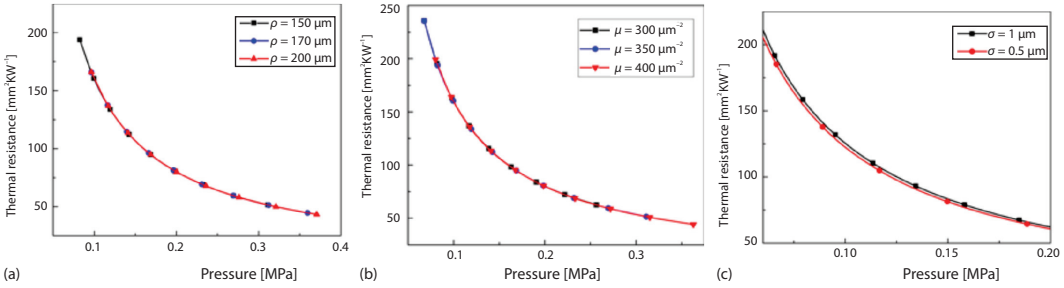

Figure 9. The influence of (a) the peak curvature, (b) the number of asperities per unit area, and (c) the standard deviation of the peak distribution on contact thermal resistance

Conclusion

A model is proposed in this paper to calculate the thermal contact resistance of VACNT, which is composed of interfacial thermal resistance, constriction thermal resistance, and VACNT resistance. The theoretical results are in good agreement with the experimental data. With the high-quality VACNT, the total thermal resistance in present model is two to three times lower than the values of the bare wafer (without CNT between Cu-Si surfaces) and the interfacial thermal resistance is the major thermal resistance. The bending degree of VACNT has important implications on the total thermal resistance. As the bending degree enhanced, the total thermal resistance will decrease gradually. When the VACNT density is determined, the contact thermal resistance can be reduced by increasing the VACNT length or by reducing the VACNT diameter. While the surface roughness exerts little effect on contact thermal resistance. By using this calculation model, it can provide more accurate parameters for optimizing the contact thermal resistance of VACNT.

Acknowledgment

This research was supported by National Key Basic Research Program of China (No. 2014CB239603)

Nomenclature

A – total contact area, [m^2]
A_e – contact area of each individual asperity, [m^2]
A_c – cross-section of CNT, [m^2]
A_n – nominal contact area, [m^2]
a – radius of the contact area, [mm]
b – radius of the heat transfer channel, [mm]
D – diameter of CNT, [nm]
d – distance between the CNT-top and the middle line of peak when CNT are uncompressed, [mm]
E – Young's modulus of CNT, [TPa]
F_0 – external contact force of the CNT with initial curvature, [N]
F_e – external contact force of each individual

asperity, [N]
h – peak height, [mm]
I – moment of inertia of the cross-section
k_c – thermal conductivity of CNT, [$Wm^{-1}K^{-1}$]
k_1, k_2 – thermal conductivities of Si and Cu surfaces, respectively, [$Wm^{-1}K^{-1}$]
L – length of CNT, [mm]
N – number of CNT per unit area contact with the asperities
N_c – total number of asperities in contact
n_i – number of CNT with different θ
P – contact pressure, [MPa]
Q – heat flux through the interface,[mm^2W^{-1}]
R_{total} – total thermal resistance, [mm^2KW^{-1}]
R_c – total constriction resistance (= $R_{cCu/CNTs}$ + $R_{cSi/CNTs}$), [mm^2KW^{-1}]
R_{CNTs} – thermal resistance of the VACNT, [mm^2KW^{-1}]
$R_{iCu/CNTs}$, $R_{iSi/CNTs}$ – interfacial thermal resistance of Cu-CNT and Si-CNT, respectively, [mm^2KW^{-1}]
r_c – individual constriction thermal resistance per unit area, [mm^2KW^{-1}]
r_i – interfacial thermal resistance of single CNT contacted with copper lattice, [mm^2KW^{-1}]
ΔT – temperature difference between the copper lattice and the CNT, [K]

Greek symbols

η – number of asperities per unit area, [mm^{-2}]
ξ – axial displacement of the CNT, [mm]
θ_0, θ – bending angle of the CNT with initial curvature, and under different force
σ_1, σ_2 – roughness of the Si and Cu surfaces, respectively, [mm]
ρ_1, ρ_2 – peak curvature of the Si and Cu surfaces, respectively, [mm]
ρ_{cnt} – density of the CNT, [mm $^{-2}$]

References

[1] Viswanath, R., *et al*., Thermal Performance Challenges from Silicon Systems, *Intel Corporation Tech. Rep*., https://pdfs.semanticscholar.org/1d27/64fc4147834a7185f1695b971e2343dfaa6b.pdf, 2000
[2] Shaikh, S., *et al*., Thermal Conductivity of an Aligned Carbon Nanotube Array, *Carbon*, *45* (2007), 13, pp. 2608-2613
[3] Xie, H., *et al*., Thermal Diffusivity and Conductivity of Multiwalled Carbon Nanotube Arrays, *Physics Letters A*, *369* (2007), 1-2, pp. 120-123
[4] Choi, T. Y., *et al*., Measurement of Thermal Conductivity of Individual Multiwalled Carbon Nanotubes by the 3-ω Method, *Applied Physics Letters*, *87* (2005), 1, 56
[5] Zhang, Y., *et al*., Compliance Properties Study of Carbon Nanofibres (CNF) Array as Thermal Interface Material, *Journal of Physics D Applied Physics*, *41* (2008), 15, 155105
[6] Zhang, K., *et al*., Carbon Nanotube Thermal Interface Material for High-Brightness Light-Emitting-Diode Cooling, *Nanotechnology*, *19* (2008), 21, 215706
[7] Zhang, G., *et al*., Temperature Dependence of Thermal Boundary Resistances between Multiwalled Carbon Nanotubes and Some Typical Counterpart Materials, *Acs Nano*, *6* (2012), 6, pp. 3057-3062
[8] Wang, H., *et al*., Reducing Thermal Contact Resistance Using a Bilayer Aligned CNT Thermal Interface Material, *Chemical Engineering Science*, *65* (2010), 3, pp. 1101-1108
[9] Khanh, H. L., *et al*., Enhancement of the Thermal Properties of a Vertically Aligned Carbon Nanotube Thermal Interface Material Using a Tailored Polymer, *Jornal of Ald Hy*, *11* (2012), 4, pp. 1-4
[10] Xu, J., Fisher, T. S., Enhancement of Thermal Interface Materials with Carbon Nanotube Arrays, *International Journal of Heat and Mass Transfer*, *49* (2006), 9, pp. 1658-1666
[11] Li, Q., *et al*., Thermal Boundary Resistances of Carbon Nanotubes in Contact with Metals and Polymers, *NanoLetters*, *9* (2009), 11, 3805
[12] Hirotani, J., *et al*., Experimental Study on Interfacial Thermal Resistance between Carbon Nanotube and Solid Material (Thermal Engineering), *Transactions of the Japan Society of Mechanical Engineers B*, *76* (2010), 769, pp. 1412-1419
[13] Kong, Q. Y., *et al*., Novel 3-D Carbon Nanotube Networks as High Performance Thermal Interface Materials, *Carbon*, *132* (2018), June, pp. 359-369
[14] Kaur, S., *et al*., Enhanced Thermal Transport at Covalently Functionalized Carbon Nanotube Array Interfaces, *Nature Communications*, *5* (2014), 2, pp. 1661-1667
[15] Sun, S., *et al*., Improving Thermal Transport at Carbon Hybrid Interfaces by Covalent Bonds, *Advanced Materials Interfaces*, *5* (2018), 15, 1800318
[16] Hu, G. J., *et al*., Thermal Resistance Between Crossed Carbon Nanotubes: Molecular Dynamics Simulations and Analytical Modelling, *Journal of Applied Physics*, *114* (2013), 22, 96

[17] Yovanovich, M. M., Four Decades of Research on Thermal Contact, Gap, and Joint Resistance in Microelectronics, *Transactions on Components and Packaging Technologies*, *28* (2005), 2, pp. 182-206
[18] Leung, M., *et al*., Prediction of Thermal Contact Conductance in Vacuum by Statistical Mechanics, *Journal of Heat Transfer*, *120* (1998), 1, pp. 51-57
[19] Ying, J., *et al*., Theoretical and Experimental Research on the Contact Thermal Resistance between Real Surface, *Journal of Zhenjiang University (Mechanical Engineering)*, *1* (1997), 1, pp. 104-109
[20] Xin, H., *et al*., Buckling and Axially Compressive Properties of Perfect and Defective Single-walled Carbon Nanotubes, *Carbon*, *45* (2007), 13, pp. 2486-2495
[21] Mesarovic, S. D., *et al.*, Mechanical Behavior of a Carbon Nanotube Turf, Scripta Materialia, *56* (2007), 2, pp. 157-160
[22] Liu, Y. Z., *Non-Linear Mechanics of Thin Elastic Rod*s, Tsinghua University Press, Beijing, China, 2006
[23] Bahrami, M., *et al.*, Thermal Contact Resistance of Non-conforming Rough Surfaces – Part 1: Contact Mechanics Model, *Journal of Thermophysics and Heat Transfer*, *18* (2004), 2, pp. 218-227
[24] Bahrami, M., *et al*., Thermal Contact Resistance of Non-conforming Rough Surfaces – Part 2: Thermal Model, *Journal of Thermophysics and Heat Transfer*, *18* (2004), 2, pp. 218-227
[25] Greenwood, J. A., Williamson, J. P., Contact of Nominally Flat Surfaces, *Proceedings of the Royal Society of London A: Mathematical*, *Physical and Engineering Sciences*, *295* (1966), pp. 300-319
[26] Chang, W. R., *et al*., An Elastic-Plastic Model for the Contact of Rough Surfaces, *Journal of Tribology*, *109* (1987), 2, pp. 257-263
[27] Huang, H., Xu, X., Effects of Surface Morphology on Thermal Contact Resistance, *Thermal Science*, *15* (2011), 5, pp. 33-38
[28] Kang, J. W., Hwang, H. J., An Ultrathin Carbon Nanoribbon Study as a Component of Nanoelectromechanical Devices, *Molecular Simulation*, *31* (2005), 8, pp. 561-565
[29] Kang, J. W., *et al*., Molecular Dynamics Study of Hypothetical Silicon Nanotubes Using the Tersoff Potential, *Journal of Nanoscience and Nanotechnology*, *2* (2002), 6, 687
[30] Saidi, P., *et al*., An Embedded Atom Method Interatomic Potential for the Zirconium-Iron System, *Computational Materials Science*, *133* (2017), June, pp. 6-13
[31] Eich, S. M., Schmitz, G., Embedded-Atom Study of Low-Energy Equilibrium Triple Junction Structures and Energies, *Acta Materialia*, *109* (2016), May, pp. 364-374
[32] Mahdavi, M. H., *et al*., Non-Linear Vibration of a Single-walled Carbon Nanotube Embedded in a Polymer Matrix Aroused by Interfacial Van Der Waals Forces, *Journal of Applied Physics*, *106* (2009), 11, 56
[33] Fuller, J. J., Marotta, E. E., Thermal Contact Conductance of Metal/Polymer Joints: An Analytical and Experimental Investigation, *Journal of Thermophysics and Heat Transfer*, *15* (2001), 2, pp. 228-238
[34] Cooper, M. G., *et al.*, Thermal Contact Conductance, *International Journal of Heat and Mass Transfer*, *12* (1969), 3, pp. 279-300
[35] Eric, P., *et al*., Thermal Conductance of an Individual Single-Wall Carbon Nanotube above Room Temperature, *Nano Letters*, 6 (2006), 1, pp. 96-100
[36] Fujii, M., *et al*., Measuring the Thermal Conductivity of a Single Carbon Nanotube, *Physical Review Letters*, *95* (2005), 6, 065502
[37] Bi, K. D., *et al*., Molecular Dynamics Simulation of Thermal Conductivity of Single-wall Carbon Nanotubes, *Physics. Letters A*., *350* (2006), 1, pp. 150-153
[38] Xu, J., Fisher, T. S., Enhanced Thermal Contact Conductance Using Carbon Nanotube Array Interfaces, *Transactions on Components and Packaging Technologies*, *29* (2006), 2, pp. 261-267

Paper submitted: June 25, 2018
Paper revised: August 7, 2018
Paper accepted: September 26, 2018